HHS Public Access

Author manuscript

Nat Chem. Author manuscript; available in PMC 2023 August 01.

Published in final edited form as:

Nat Chem. 2022 August ; 14(8): 891–897. doi:10.1038/s41557-022-00937-w.

A two-directional vibrational probe reveals different electric field orientations in solution and an enzyme active site

Chu Zheng[1,3], **Yuezhi Mao**[1,3], **Jacek Kozuch**[2], **Austin O. Atsango**[1], **Zhe Ji**[1], **Thomas E. Markland**[1], **Steven G. Boxer**[1]

[1]Department of Chemistry, Stanford University, Stanford, CA, USA.

[2]Experimental Molecular Biophysics, Department of Physics, Freie Univeresität Berlin, Berlin, Germany.

[3]These authors contributed equally: Chu Zheng, Yuezhi Mao.

Abstract

The catalytic power of an electric field depends on its magnitude and orientation with respect to the reactive chemical species. Understanding and designing new catalysts for electrostatic catalysis thus requires methods to measure the electric field orientation and magnitude at the molecular scale. We demonstrate that electric field orientations can be extracted using a two-directional vibrational probe by exploiting the vibrational Stark effect of both the C═O and C—D stretches of a deuterated aldehyde. Combining spectroscopy with molecular dynamics and electronic structure partitioning methods, we demonstrate that, despite distinct polarities, solvents act similarly in their preference for electrostatically stabilizing large bond dipoles at the expense of destabilizing small ones. In contrast, we find that for an active-site aldehyde inhibitor of liver alcohol dehydrogenase, the electric field orientation deviates markedly from that found in solvents, which provides direct evidence for the fundamental difference between the electrostatic environment of solvents and that of a preorganized enzyme active site.

Correspondence and requests for materials should be addressed to Thomas E. Markland or Steven G. Boxer. tmarkland@stanford.edu; sboxer@stanford.edu.

Author contributions

C.Z. and S.G.B. designed the research. C.Z. performed the experiments and fixed-charge MD simulations. Y.M. developed the computational protocol that combined MD simulations and QM calculations to quantify the solvent electric field contributions, implemented the electronic structure partitioning schemes in the Q-Chem software package and performed the QM calculations. J.K. performed the AMOEBA polarizable MD simulations. A.O.A. analysed the data from the MD simulations and wrote the codes to extract the truncated solute–solvent structures for the QM calculations. Z.J. synthesized *N*-[formyl-^{2}H]cyclohexylformamide. C.Z., Y.M., T.E.M. and S.G.B. discussed the results and wrote the manuscript. All the authors contributed to improving the manuscript.

Competing interests

The authors declare no competing interests.

Online content

Any methods, additional references, Nature Research reporting summaries, source data, extended data, supplementary information, acknowledgements, peer review information; details of author contributions and competing interests; and statements of data and code availability are available at https://doi.org/10.1038/s41557-022-00937-w.

Supplementary information The online version contains supplementary material available at https://doi.org/10.1038/s41557-022-00937-w.

The physical basis for the remarkable proficiency and specificity of enzymes under mild physiological conditions has been widely debated. One essential contribution is electrostatic preorganization[1,2], the precise positioning of functional groups with charges and dipoles by the protein scaffold that preferentially stabilizes the transition state (TS) over the reactant state (RS) due to the electric field at the active site, which leads to a decrease in the activation free energy barrier (Fig. 1a). This mechanism is directly supported by studies of several model enzymes[2-7], among which a prime example is ketosteroid isomerase[8,9], in which a large electric field (about −150 MV cm^{-1}) exerted by functional groups at the active site was measured, which leads to an about 10^5-fold rate of acceleration and accounts for a large fraction of the reduction in the activation free energy compared with that of the same reaction in water. Electric fields can be measured by exploiting the vibrational Stark effect (VSE), in which the infrared or Raman frequency shifts are related to the projection of the field on a particular bond. This is accomplished by using VSE probes calibrated via a combination of vibrational Stark spectroscopy (VSS), vibrational solvatochromism and molecular dynamics (MD) simulations[2,8,10,11].

The concept of electrostatic preorganization is illustrated in Fig. 1b, which compares a reaction that involves charge reorganization occurring in water to that at the active site of an enzyme. As solvent molecules, such as water, fluctuate around the reactant to stabilize the RS dipole moment on average, solvent configurations that stabilize the TS are rare and thus require substantial reorganization in the course of a reaction. In contrast, an electrostatically preorganized catalyst active site requires minimal adjustments to preferentially stabilize the charge distribution in the TS, and thus minimizes the reorganization energy[1]. Although this viewpoint is supported by computational studies[1,12-19], there is limited direct experimental evidence for the critical assumption that the electric field orientation experienced by a substrate at enzyme active sites differs from that in solvents. The challenge to experimentally test this hypothesis lies in the fact that most previous studies only measured the projection of the electric fields along one chemical bond at a time, and even when this is the bond involved in the catalysis, it only provides information on the magnitude of the projected electric field, but not on the orientation of the total field.

In this work, we directly measured the orientation of electric fields in condensed-phase environments using a vibrational probe that bore two chemical bonds whose vibrational frequencies were both markedly shifted by the electric fields that arose from their chemical environments, which allowed us to measure the fields experienced by this probe along two directions (Fig. 1c). Using the deuterated (aldehyde H) form of *N*-cyclohexylformamide (CXF-D; Fig. 1d), a liver alcohol dehydrogenase (LADH) inhibitor[20,21], we obtained the projections of the electric field that arose from the solvents and LADH active site on both the carbonyl (C═O) and carbon–deuterium (C–D) bonds that are approximately 120° from each other (Fig. 1c). Intriguingly, we found that the vibrational frequencies of C═O ($\nu_{C=O}$) and C—D ($\nu_{C\text{-}D}$) shifted in opposite directions as the solvent polarity increased, which indicated the coexistence of stabilization (C═O) and destabilization (C—D) of the chemical bonds around a single atom in solution. To elucidate these observations and introduce a field-frequency map for this probe in complex condensed phase environments, such as enzyme active sites, we developed a computational framework that combined

MD simulations with recently introduced electronic structure partitioning methods[22,23], which gives an improved accuracy and reliability in predicting the solvent electric fields compared with those of previously available methods. For a wide range of solvents, we observed a strong correlation between the electric fields experienced by the C═O and C—D bonds, which suggests that different solvents, despite their diverse chemical structures and polarities, exert electric fields of a similar orientation on the aldehyde moiety. By contrast, at the active site of LADH, we reveal that the aldehyde moiety, which participates in the enzyme-catalysed reaction, experienced a substantially different electric field orientation. This provides direct evidence for the intrinsic differences between the electrostatic environments of solvents and an enzyme active site experienced by a chemically relevant species.

Results and discussion

Experimental validation of two-directional electric field measurements by vibrational Stark spectroscopy.

The infrared absorption spectra for the C—D and C═O stretches in CXF-D are shown in Fig. 2a,b, respectively. Although the absorbance of the C—D stretch is typically ~100 times weaker than that of the C═O (or C≡N) stretch[24], the single C—D stretch in CXF-D shows a reasonably large extinction coefficient (ε_{max}≈3 M^{-1} cm^{-1}, which is about 1/30th that of C═O), which facilitates its application as a VSE probe. To validate the spectroscopic response of C═O and C—D in CXF-D to an external electric field, we used VSS, in which an external electric field of known magnitude (~1.0 MV cm^{-1}) was applied to the sample in a frozen glass (Fig. 2). The Stark spectrum is dominated by the second-derivative band shape from which the Stark tuning rates, $|\Delta\mu_{C=O}|f_{C=O} = 1.13 \pm 0.01\,cm^{-1}\,(MV\,cm^{-1})^{-1}$ and $|\Delta\mu_{C-D}|f_{C-D} = 1.32 \pm 0.04\,cm^{-1}\,(MV\,cm^{-1})^{-1}$, were obtained (see Supplementary Fig. 1 and Supplementary Table 1 for details of the fitting). The Stark tuning rate we obtained for the aldehyde carbonyl is in good agreement with the reported values for other carbonyl compounds[3,11], and the values for both C═O and C—D can be well reproduced (1.01 and 1.22 cm^{-1} (MV^{-1} cm^{-1}), respectively) using ‘Stark in silico’ calculations, in which we performed ab initio frequency calculations with an external electric field applied along the bond directions while treating the solvent as a dielectric continuum (Supplementary Method 13, Supplementary Text 3 and Supplementary Table 30). Here $f_{C=O}$ and $f_{C\text{-}D}$ are scalar approximations of the local field factors[25] in the directions of the C═O and C—D bonds, respectively. The local field factor is a tensor that describes the difference between the externally applied electric field and the actual electric field experienced by VSE probes and could be different for the C═O and C—D stretches[10,25] (Supplementary Text 3). Although the sign of the Stark tuning rates cannot be explicitly determined by VSS as the sample is isotropic, for vibrational transitions the Stark tuning rates should be positive in most cases because the excited-state dipole moment is expected to be larger than that of the ground state due to vibrational anharmonicity. The dominance of the second-derivative band shape in the Stark spectra (Fig. 2c,d) indicates that the frequency shifts of both the C═O and C—D stretch modes in response to an external electric field are primarily determined by the linear VSE[26]. Similar VSS results were also found for methyl formate-D, a different compound

that also carries a deuterated aldehyde group (Supplementary Fig. 2), which demonstrates the generality of using a deuterated aldehyde to probe electric fields in two directions.

Opposite frequency shifts of C═O and C—D bonds upon solvation.

Figure 3 shows that $\nu_{C=O}$ and $\nu_{C\text{-}D}$ exhibit frequency shifts in opposite directions upon increasing the solvent polarity, a trend that is also observed for methyl formate-D (Supplementary Fig. 3). Although it has been widely observed that vibrational probes, such as C═O and C≡N, undergo redshifts with increasing solvent polarity[27], for this vibrational probe two bonds that arise from the same atom show frequency shifts in opposite directions, where C—D exhibits a blueshift and C═O a redshift. As shown below, this arises because solvent tends to organize around the more polar C═O bond due to attractive electrostatic interactions, resulting in a redshift, which in turn leads to destabilizing interactions sensed by the C—D bond at an about 120° angle from the C═O direction.

Evaluation of the solvent electric fields on C═O and C—D bonds using molecular simulation.

To unravel the origins of this unusual solvatochromic behaviour, we performed MD simulations and quantum mechanical (QM) electronic structure calculations to quantify the solvent electric fields projected on the C═O and C—D bonds. Although fixed-charge MD simulations have been successfully used to establish field-frequency maps for C═O in various compounds[3,8,10,11,28], the map produced for C—D using this method provides a poor correlation between the experimentally observed frequency shifts and the calculated fields (Supplementary Fig. 4). To more accurately quantify the fields experienced by the C—D probe, we therefore adapted two recently developed electronic structure partitioning schemes[22,23] to obtain more accurate solvent electric fields for configurations obtained from MD sampling. The QM-based approach can significantly improve the accuracy of field calculations because it avoids the use of any parameters assigned by the force field, such as atomic charge or polarizability, but instead obtains the electric field directly from the electrostatic potential created by electrons and nuclei in the system. As shown in Supplementary Tables 6-12, the results obtained from both SPADE[22] (subsystem projected AO decomposition)- and ALMO[23] (absolutely localized molecular orbitals)-based partitioning schemes gave consistent predictions of the solvent electric fields when combined with solvent configurations obtained from either fixed-charge[11] or polarizable force fields[28,29]. This approach thus provides a reliable way to quantify the solvent electric fields projected onto the vibrational probes, which enabled us to uncover the physical origin of the unusual solvatochromic shifts as well as to establish the field-frequency map for CXF-D.

Figure 4a,b shows that for both C—D and C═O, over a wide range of solvent polarities (dielectric constants from 1 to 80), there is a strong linear correlation between the ensemble-averaged solvent electric fields obtained from our simulations and the experimentally measured frequencies. The ensemble-averaged solvent electric field along the C═O bond is negative, which has also been found for many other carbonyl-containing molecules[3,11,28]. The negative electric field along the C═O bond signifies an attractive electrostatic interaction with solvents because the field is aligned with the bond dipole, which lies in

the O → C direction. In contrast, the C—D bond in CXF-D has a more subtle dipole moment in which both C and D are positively charged, but C is more so (Supplementary Table 27), which gives a dipole in the D → C direction. The electric field along the C—D bond is positive and thus antiparallel with the bond dipole direction, which indicates that the electrostatic interaction with the solvent destabilizes the C—D covalent bond, consistent with the blueshift observed in its vibrational frequency as the solvent polarity increases. The correlation between the experimental frequency shifts and calculated fields thus provides strong support that the electrostatic interactions are responsible for modulating the vibrational frequencies. We note that the linearity of the correlation for C—D is not as good as that for C═O (R^2 = 0.83 versus 0.99). This most likely arises due to a Fermi resonance between the C—D stretch and the overtone of C—D bending modes that appears as a shoulder peak at around 2,100 cm^{-1} (Supplementary Text 5 and Supplementary Table 31), consistent with previous studies on the vibrational spectra of aldehydes[30]. To further validate our computational procedure, we also performed ‘Stark in silico’ calculations in vacuum with an external electric field applied along the C═O or C—D direction, from which we observed a strong correlation between the strength of the applied field and the computed C═O and C—D frequencies (Supplementary Fig. 5 and Supplementary Table 14).

The stark contrast in the solvent electric field directions on C═O and C—D manifests how these two bonds, connected to a common atom centre, interact with the solvents. As C═O has a substantially larger bond dipole than C—D (Supplementary Table 27), it is preferentially stabilized by the solvent, via both the local arrangements of the solvent molecules and their electronic polarization (Supplementary Fig. 17). Owing to the ~120° angle between the C═O and C—D bonds, the field induced by the solvent ordering around C═O causes C—D to experience a field that is opposite to its bond dipole direction, which results in its destabilization. To further corroborate this physical picture, we performed simulations of *N*-cyclohexylacetamide (Supplementary Table 15), in which the deuterium atom in CXF-D is replaced by a methyl group and thus removes any specific interactions that may exist between C—D and the solvent molecules. In this methylated analogue, we observed that the positive field along the C—C(methyl) bond, which is in the same direction as C—D, is largely retained (reduced by ~20%) and thus confirms that the positive electric field along C—D is a secondary effect due to the preferential stabilization of C═O. This picture of preferential stabilization of the more polar C═O group provides additional details about the solute–solvent interactions that are not captured by the Onsager reaction field model[31], one of the most widely used models for solvation based on the concept that globally the molecular dipole of a solute experiences a stabilizing reaction field. Our results show clear evidence that locally, that is, at the level of individual chemical bonds[32], there are both stabilizing and destabilizing electrostatic interactions experienced by solute molecules in solutions. Given its electrostatic origin, the trend in the opposite frequency shifts of C═O and C—D upon increasing solvent polarity can be qualitatively captured using a simple polarizable continuum model[33] for the solvents (Supplementary Table 16); however, a quantitative description of the solvatochromic effects necessitates considering the specific molecular ordering of the solvent around the probe.

To further elucidate the competition between the C═O and C—D dipoles in organizing the solvent around them, we examined the solvatochromic behaviour of the carbonyl group in acetyl chloride, in which the C—D is replaced by the much more polar carbon–chlorine (C—Cl) bond. In this case, C—Cl can much more effectively compete with C═O for solvent organization, resulting in negative (stabilizing) electric fields along both bonds with the magnitude of that along C═O reduced notably (Supplementary Fig. 12). Remarkably, we found that the C═O of acetyl chloride showed only a 2 cm^{-1} redshift going from hexane to acetonitrile (acetyl chloride is not stable in water), a much smaller solvent shift than that of CXF-D (19 cm^{-1}) or any other carbonyl-containing molecule observed to date (Supplementary Fig. 7 and Supplementary Table 17). Given that the C═O of acetyl chloride has a typical Stark tuning rate as obtained from both VSS experiments and 'Stark *in silico*' calculations (Supplementary Fig. 8, Supplementary Table 1 and 18), this extraordinarily small solvation redshift indicates that the C═O of acetyl chloride, unlike that of CXF-D, gains a much lesser degree of electrostatic stabilization as the solvent polarity increases (Supplementary Text 1). The observation that the C—Cl bond suppresses the preferential stabilization of C═O by the solvent in acetyl chloride further underlines the ubiquity of distinct local solvation effects governed by bond dipoles, which may have far-reaching implications in, for example, small-molecule catalyst design.

Probing the active-site electric field of LADH.

LADH catalyses a hydride transfer reaction, which is ubiquitous in many metabolic pathways, for the interconversion between alcohol and aldehyde using NAD^+ or NADH as the redox cofactor[34]. To probe the magnitude and orientation of the electric fields in wild-type LADH, we introduced the CXF-D probe, which serves as an aldehyde-analogue inhibitor, to its active site. As shown in Fig. 5a,b, this leads to red- and blueshifts in the C═O and C—D frequencies, respectively, which are even larger ($\nu_{C=O} = 1,618\,cm^{-1}$ and $\nu_{C\text{-}D} = 2,218\,cm^{-1}$) than those in water ($\nu_{C=O} = 1,627\,cm^{-1}$ and $\nu_{C-D} = 2,182\,cm^{-1}$), the most polar solvent that we investigated (Supplementary Fig. 9 and Supplementary Tables 19 and 20). In addition, the linewidths of both the C═O and C—D spectra in the enzyme were much narrower than those in water, probably due to the smaller range of fluctuations possible in the active-site environment, as has been observed in many enzymes[2]. Based on the field-frequency maps for CXF-D that we obtained using a wide range of solvents (Fig. 4), the measured frequency shifts indicated that the active-site electric field projected on C═O was −166 MV cm^{-1}, whereas that on C—D was +99 MV cm^{-1}, which are both larger in magnitude than the average values observed in any of the solvents. CXF-D's C═O, similar to that of the substrate in aldehyde reduction reactions, is known to strongly interact with Ser-48 and Zn^{2+} at the active site[20,21] (Fig. 1 and Supplementary Fig. 10). Hence these specific interactions are the most likely sources of the large active-site electric field. In contrast, based on the crystal structure we obtained at 1.43 Å (Supplementary Fig. 10), the C—D in CXF-D does not interact strongly with the nearby residues, which suggests that the main contributions to its large positive electric field are from Ser-48 and Zn^{2+}, which preferentially stabilize C═O and destabilize C—D as a secondary effect.

Comparison of the electric field orientation at the LADH active site to that in the solvents.

As shown in Fig. 5c, there is a strong linear correlation (R^2 = 0.93) between the average electric fields projected on C═O and C—D for CXF-D in the solvents. Despite the substantial changes in the electric field magnitudes across the solvents due to their diverse polarities, the ratio between the average solvent electric field projected on C═O ($F_{C=O}$) and C—D (F_{C-D}) remains essentially unchanged at $F_{C-D} / F_{C=O} = -0.39 \pm 0.02$. Using this ratio and assuming that the angle between the C═O and C—D groups is fixed at 120° for the sp^2 carbon we extracted the orientation of the electric field vector in the aldehyde plane, namely its angle to the bond dipole direction of C═O, labelled θ in Fig. 1c. This angle was shown (Supplementary Text 2) to be given by:

$$\theta = \arctan\left[\frac{1}{\sqrt{3}}\left(1 + 2\frac{F_{C-D}}{F_{C=O}}\right)\right]. \quad (1)$$

Therefore, the nearly constant value of $F_{C-D} / F_{C=O}$ across all the solvents indicates that the electric field orientations in the aldehyde plane were remarkably similar. This finding is further supported by the results in other polar protic solvents besides water (methanol and ethanol; Supplementary Text 4 and Supplementary Figs. 15 and 16) and implies that, despite their distinct chemical structures and polarities[35], all these solvents tend to organize in a similar way to electrostatically stabilize the solute (vibrational probe). From the average value of this ratio we obtained an angle θ of 7.2 ± 1.3°, that is, the electric field was almost parallel to the C═O bond dipole and pointed slightly away from C—D (Fig. 5d). This small value of θ further supports the physical picture that the solvents preferentially stabilize C═O, and the small deviation from being exactly parallel (0°) may be beneficial to stabilize the solute globally by reducing the destabilization of C—D compared with that of a field that is perfectly parallel with the C═O bond dipole.

In contrast, the electric field at the active site of LADH is oriented differently in the aldehyde plane as compared with that in the solvents. Using the $F_{C=O}$ and F_{C-D} values for LADH (−166 and +99 MV cm^{-1}, respectively) and equation (1), the angle θ obtained is −6.4°. This angle corresponds to the electric field vector experienced by the aldehyde group of CXF-D being slightly skewed towards the opposite side of the C═O bond dipole direction, that is, towards C—D, compared with that in the solvents in which it is away from C—D (Fig. 5d). Hence, in the two-dimensional plane of the aldehyde moiety the electric field orientation at the LADH active site is rotated by ~14° relative to that in the solvents, which leads to a field orientation that enhances the positive field projection along the C—D bond and thus further destabilizes it. This provides experimental evidence that unlike solvents whose organization around the solute is largely directed by the solute bond dipoles to achieve a global electrostatic stabilization, the enzyme active site is preorganized, which tunes the relative stabilization of the aldehyde moiety's C═O and C—D bonds by imposing a distinct electric field on the reactive chemical moiety (the aldehyde group) that is rarely accessible in solvents in terms of both magnitude and orientation.

Conclusions

In summary, we have introduced an approach based on the VSE to measure both the magnitude and orientation of the electric fields in condensed phase systems. By exploiting a two-directional vibrational probe, CXF-D, we showed that its deuterated aldehyde group can be calibrated using experiments and a computational framework based on MD and electronic structure calculations to report the electric field strengths along both the C═O and C—D directions. Using this probe, we demonstrated the coexistence of stabilizing and destabilizing electrostatic interactions experienced by the individual chemical bonds of a solute in a wide range of solvents, as well as the nearly invariant field orientation across solvents of distinct chemical structures and polarities. This provides direct experimental insights into how local solvent organization around a solute molecule driven by the difference in bond dipoles affords global electrostatic stabilization. In contrast, we showed that the electric field at the active site of LADH, as measured by the CXF-D probe, possesses a markedly different orientation that provides a greater electrostatic destabilization of the C—D bond than that observed in the solvents. Hence, although the electric fields at an enzyme's active site and in aqueous solutions may be of comparable magnitudes, the orientations of these fields are intrinsically different. This supports the hypothesis that enzymes may provide preorganized electrostatic environments that maximize their catalytic power[1,2]. Finally, the experimental and computational framework that we introduce here to probe electric field orientations using deuterated aldehydes can be widely applied to other systems in complex environments and with complex solutes, including homogeneous catalysts, and thus serves as a prototype for the characterization of electric field orientations to stimulate future investigations on the functional role of field orientation in enzymatic and electrostatic catalysis.

Supplementary Material

Refer to Web version on PubMed Central for supplementary material.

Acknowledgements

We express our gratitude to B. V. Plapp at the University of Iowa for providing detailed guidance on the expression and purification of LADH and much other valuable advice. We thank C.-Y. Lin for his help with X-ray crystallography, S. Schneider, J. Weaver, J. Kirsh and S. D. E. Fried for helpful discussions, T. Carver at the Stanford Nano Shared Facilities for nickel coating the Stark windows, T. McLaughlin from Stanford University Mass Spectrometry (SUMS) for technical support with the mass spectrometry. C.Z. is grateful for the Stanford Center for Molecular Analysis and Design (CMAD) Fellowship. J.K. acknowledges support from the German Research Foundation DFG-Project-ID221545957-SFB1078/B9. This work was supported in part by NIH Grant GM118044 (to S.G.B.) and the National Science Foundation grant no. CHE-1652960 (to T.E.M.). T.E.M. also acknowledges support from the Camille Dreyfus Teacher-Scholar Awards Program. Use of the Stanford Synchrotron Radiation Lightsource, SLAC National Accelerator Laboratory, is supported by the US Department of Energy, Office of Science, Office of Basic Energy Sciences under contract no. DE-AC02-76SF00515. The SSRL Structural Molecular Biology Program is supported by the DOE Office of Biological and Environmental Research, and by the National Institutes of Health, National Institute of General Medical Sciences (P30GM133894). The contents of this publication are solely the responsibility of the authors and do not necessarily represent the official views of NIGMS or NIH. This research also used resources of the National Energy Research Scientific Computing Center (NERSC), a US Department of Energy Office of Science User Facility operated under contract no. DE-AC02-05CH11231, and the Sherlock cluster operated by the Stanford Research Computing Center.

Data availability

The gene sequence for the wild-type enzyme in this study has been deposited in GenBank (accession code OM863576). The X-ray coordinates and structural factors have been deposited in the Protein Data Bank as entry 7RM6 for the wild-type enzyme in complex with NADH and CXF. The electronic structure partitioning methods for DFT calculations of solvent electric fields at atomic positions were implemented in the Q-Chem software package[36], which is available in the 5.4.2 and later releases. Source data are provided with this paper. All the data that support the finding of this study are available within this article and its Supplementary Information and available on Figshare (https://doi.org/10.6084/m9.figshare.19248108).

Code availability

The code used for processing MD trajectories and calculating electric field projections along bond directions is available at https://github.com/YuezhiMao/2D_VSE_probe and Zenodo (https://zenodo.org/record/6300009#.Yhw0GBPMKS4)

References

1. Warshel A et al. Electrostatic basis for enzyme catalysis. Chem. Rev 106, 3210–3235 (2006). [PubMed: 16895325]
2. Fried SD & Boxer SG Electric fields and enzyme catalysis. Annu. Rev. Biochem 86, 387–415 (2017). [PubMed: 28375745]
3. Schneider SH & Boxer SG Vibrational Stark effects of carbonyl probes applied to reinterpret IR and Raman data for enzyme inhibitors in terms of electric fields at the active site. J. Phys. Chem. B 120, 9672–9684 (2016). [PubMed: 27541577]
4. Carey PR Spectroscopic characterization of distortion in enzyme complexes. Chem. Rev 106, 3043–3054 (2006). [PubMed: 16895317]
5. Dong J et al. The strength of dehalogenase–substrate hydrogen bonding correlates with the rate of Meisenheimer intermediate formation. Biochemistry 42, 9482–9490 (2003). [PubMed: 12899635]
6. Tonge PJ & Carey PR Length of the acyl carbonyl bond in acyl-serine proteases correlates with reactivity. Biochemistry 29, 10723–10727 (1990). [PubMed: 2271679]
7. Deng H et al. Source of catalysis in the lactate dehydrogenase system. Ground-state interactions in the enzyme-substrate complex. Biochemistry 33, 2297–2305 (1994). [PubMed: 8117687]
8. Fried SD, Bagchi S & Boxer SG Extreme electric fields power catalysis in the active site of ketosteroid isomerase. Science 346, 1510–1514 (2014). [PubMed: 25525245]
9. Wu Y & Boxer SG A critical test of the electrostatic contribution to catalysis with noncanonical amino acids in ketosteroid isomerase. J. Am. Chem. Soc 138, 11890–11895 (2016). [PubMed: 27545569]
10. Fried SD & Boxer SG Measuring electric fields and noncovalent interactions using the vibrational stark effect. Acc. Chem. Res 48, 998–1006 (2015). [PubMed: 25799082]
11. Fried SD, Bagchi S & Boxer SG Measuring electrostatic fields in both hydrogen-bonding and non-hydrogen-bonding environments using carbonyl vibrational probes. J. Am. Chem. Soc 135, 11181–11192 (2013). [PubMed: 23808481]
12. Wu Y, Fried SD & Boxer SG A preorganized electric field leads to minimal geometrical reorientation in the catalytic reaction of ketosteroid isomerase. J. Am. Chem. Soc 142, 9993–9998 (2020). [PubMed: 32378409]
13. Welborn VV & Head-Gordon T Computational design of synthetic enzymes. Chem. Rev 119, 6613–6630 (2019). [PubMed: 30277066]

14. Welborn VV, Pestana LR & Head-Gordon T Computational optimization of electric fields for better catalysis design. Nat. Catal 1, 649–655 (2018).
15. Fuxreiter M & Mones L The role of reorganization energy in rational enzyme design. Curr. Opin. Chem. Biol 21, 34–41 (2014). [PubMed: 24769299]
16. Kamerlin SC, Sharma PK, Chu ZT & Warshel A Ketosteroid isomerase provides further support for the idea that enzymes work by electrostatic preorganization. Proc. Natl Acad. Sci. USA 107, 4075–4080 (2010). [PubMed: 20150513]
17. Bím D & Alexandrova AN Electrostatic regulation of blue copper sites. Chem. Sci 12, 11406–11413 (2021). [PubMed: 34667549]
18. Shaik S, Mandal D & Ramanan R Oriented electric fields as future smart reagents in chemistry. Nat. Chem 8, 1091–1098 (2016). [PubMed: 27874869]
19. Xu L, Izgorodina EI & Coote ML Ordered solvents and ionic liquids can be harnessed for electrostatic catalysis. J. Am. Chem. Soc 142, 12826–12833 (2020). [PubMed: 32610899]
20. Deng H, Schindler JF, Berst KB, Plapp BV & Callender R A Raman spectroscopic characterization of bonding in the complex of horse liver alcohol dehydrogenase with NADH and *N*-cyclohexylformamide. Biochemistry 37, 14267–14278 (1998). [PubMed: 9760265]
21. Ramaswamy S, Scholze M & Plapp BV Binding of formamides to liver alcohol dehydrogenase. Biochemistry 36, 3522–3527 (1997). [PubMed: 9132002]
22. Claudino D & Mayhall NJ Automatic partition of orbital spaces based on singular value decomposition in the context of embedding theories. J. Chem. Theory Comput 15, 1053–1064 (2019). [PubMed: 30620604]
23. Khaliullin RZ, Head-Gordon M & Bell AT An efficient self-consistent field method for large systems of weakly interacting components. J. Chem. Phys 124, 204105 (2006). [PubMed: 16774317]
24. Adhikary R, Zimmermann J & Romesberg FE Transparent window vibrational probes for the characterization of proteins with high structural and temporal resolution. Chem. Rev 117, 1927–1969 (2017). [PubMed: 28106985]
25. Bublitz GU & Boxer SG Stark spectroscopy: applications in chemistry, biology, and materials science. Annu. Rev. Phys. Chem 48, 213–242 (1997). [PubMed: 9348658]
26. Boxer SG Stark realities. J. Phys. Chem. B 113, 2972–2983 (2009). [PubMed: 19708160]
27. Baiz CR et al. Vibrational spectroscopic map, vibrational spectroscopy, and intermolecular interaction. Chem. Rev 120, 7152–7218 (2020). [PubMed: 32598850]
28. Kozuch J et al. Testing the limitations of MD-based local electric fields using the vibrational Stark effect in solution: penicillin G as a test case. J. Phys. Chem. B 125, 4415–4427 (2021). [PubMed: 33900769]
29. Fried SD, Wang LP, Boxer SG, Ren P & Pande VS Calculations of the electric fields in liquid solutions. J. Phys. Chem. B 117, 16236–16248 (2013). [PubMed: 24304155]
30. Eggers DF & Lingren WE C—H vibrations in aldehydes. Anal. Chem 28, 1328–1329 (1956).
31. Onsager L Electric moments of molecules in liquids. J. Am. Chem. Soc 58, 1486–1493 (1936).
32. Levinson NM, Fried SD & Boxer SG Solvent-induced infrared frequency shifts in aromatic nitriles are quantitatively described by the vibrational Stark effect. J. Phys. Chem. B 116, 10470–10476 (2012). [PubMed: 22448878]
33. Tomasi J, Mennucci B & Cammi R Quantum mechanical continuum solvation models. Chem. Rev 105, 2999–3093 (2005). [PubMed: 16092826]
34. Sekhar VC & Plapp BV Rate constants for a mechanism including intermediates in the interconversion of ternary complexes by horse liver alcohol dehydrogenase. Biochemistry 29, 4289–4295 (1990). [PubMed: 2161681]
35. Reichardt C & Welton T Solvents and Solvent Effects in Organic Chemistry (John Wiley & Sons, 2011).
36. Epifanovsky E et al. Software for the frontiers of quantum chemistry: an overview of developments in the Q-Chem 5 package. J. Chem. Phys 155, 084801 (2021). [PubMed: 34470363]

37. Johnson RD III NIST Computational Chemistry Comparison and Benchmark Database. NIST Standard Reference Database Number 101, Release 21 August 2020 (NIST, accessed 2 January 2021).

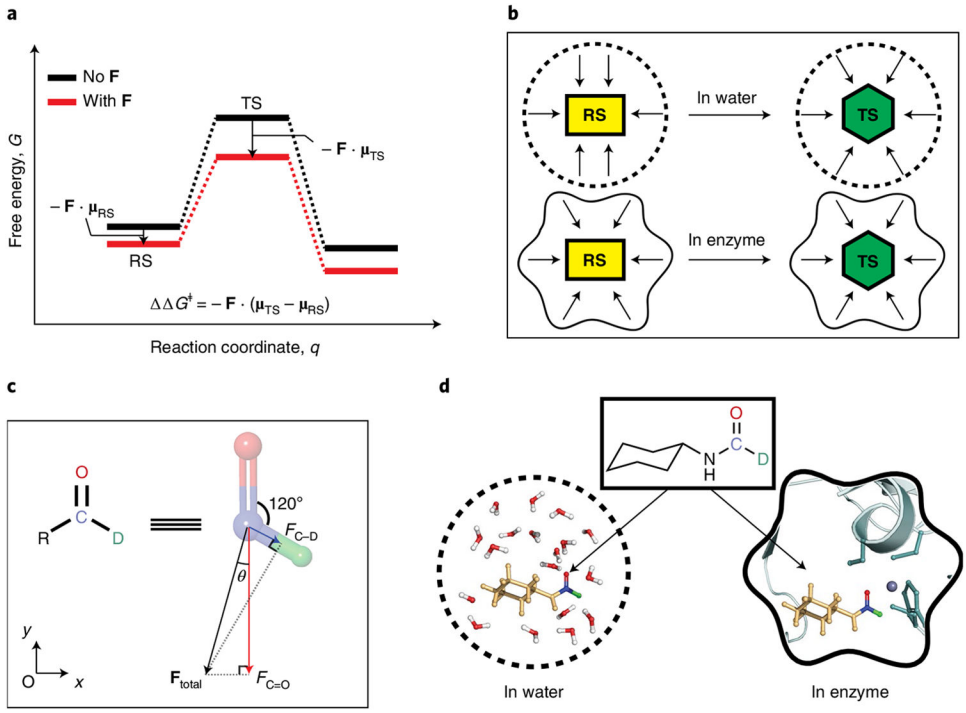

Fig. 1 | Electrostatic catalysis and the two-directional vibrational probe used in this work. **a**, The model of electrostatic catalysis in enzymes: the reaction barrier is reduced by preferential stabilization of the TS because of the preorganized electric field, **F**, at the active site. **b**, Schematic illustration of the environmental response to the formation of the TS from RS during a chemical reaction that involves charge displacement (from rectangular to hexagonal for illustrative purposes). The top row illustrates the solvent reorganization in water (arrows represent the solvent dipoles), which contrasts with the minimal change in electric field orientation at the active site of enzymes due to electrostatic preorganization in the bottom row. **c**, The concept of probing the orientation of an electric field by using the C═O and C—D stretch vibrations of an aldehyde. The total electric field on the two-dimensional plane of the aldehyde moiety is the vector sum of the fields measured along the two directions. **d**, The structure of the VSE probe CXF-D used in this article to measure the electric field orientations in solvents (left) and at the active site of LADH (right). The crystal structure of the wild-type LADH in complex with NADH and CXF was resolved at 1.43 Å (Protein Data Bank: 7RM6).

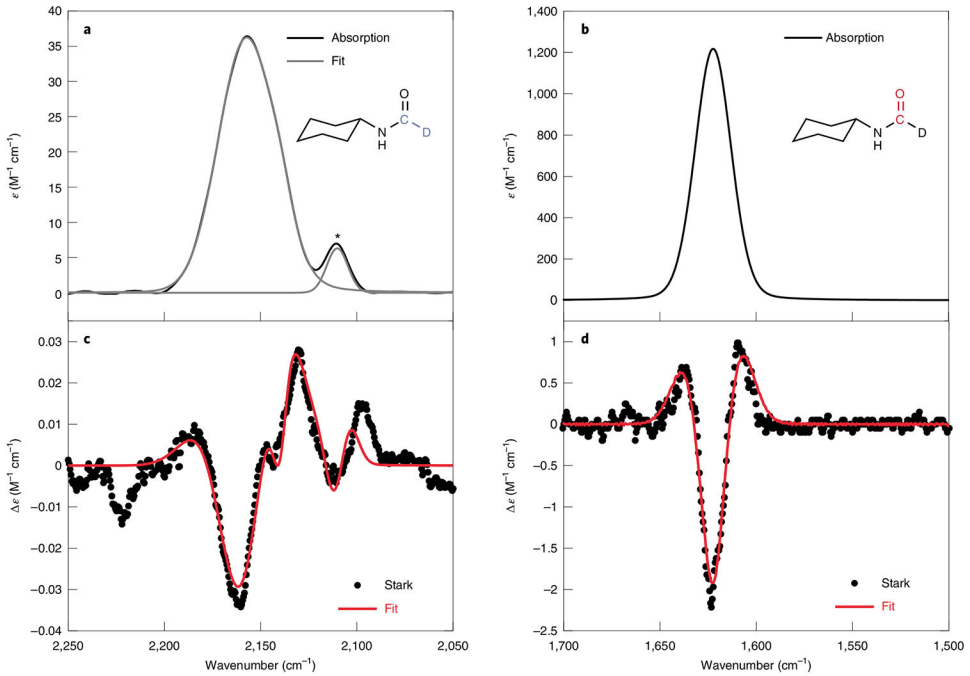

Fig. 2 |. Infrared absorption and Stark spectra of CXF-D at 77 K demonstrating the VSEs of the C—D (left) and C═O (right) bonds.

a–**d**, Infrared absorption spectra (**a**,**b**) and the corresponding vibrational Stark spectra scaled to an applied field of 1.0 MV cm^{-1} with best fits (red lines) (**c**,**d**). See Supplementary Fig. 1 and Supplementary Table 1 for the fitting details. The small shoulder peak labelled with an asterisk at around 2,100 cm^{-1} in **a** is most likely due to a Fermi resonance (Supplementary Text 5 and Supplementary Table 31). The C—D stretch was measured in 2-methyltetrahydrofuran and the C═O stretch in D_2O/glycer(ol-D_3) (v/v 1:1). Different solvents were used because the C═O stretch of CXF-D shows multiple bands in 2-methyltetrahydrofuran, which most likely arise from dimerization due to intermolecular hydrogen bonds.

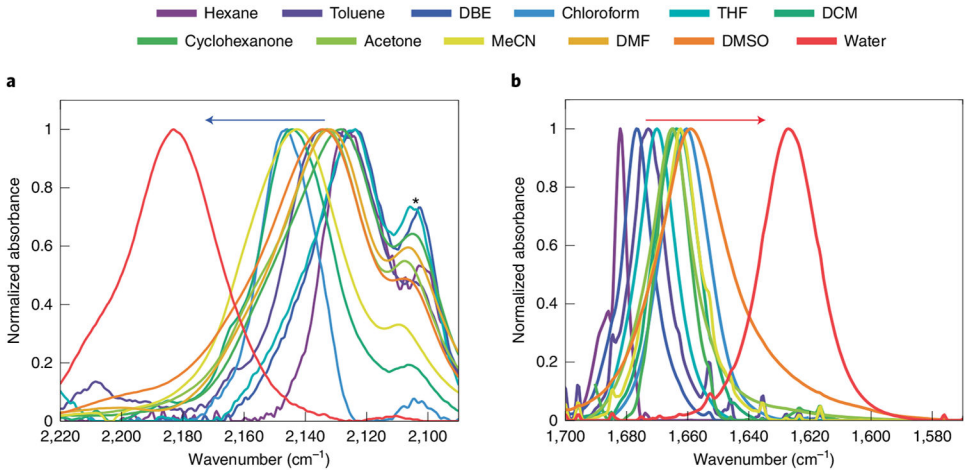

Fig. 3 | Normalized infrared spectra of CXF-D in a series of solvents with various polarities. **a**,**b**, The spectra demonstrate the solvatochromic shifts in the C—D (**a**) and C═O (**b**) frequencies. The concentrations of CXF-D in the measurements for ν_{C-D} and $\nu_{C=O}$ were 20 and 1 mM, respectively. The blue and red arrows indicate the direction of the frequency shifts of C—D and C═O, respectively, with the increase in solvent polarity. The small shoulder peak labelled with an asterisk at around 2,100 cm^{-1} in **a** is most likely due to a Fermi resonance, which is evidenced by its minimal frequency shift with different solvents and yet a more pronounced change in intensity as the C—D stretch band shifts. DBE, dibutyl ether; THF, tetrahydrofuran; DCM, dichloromethane; MeCN, acetonitrile; DMF, dimethylformamide; DMSO, dimethylsulfoxide.

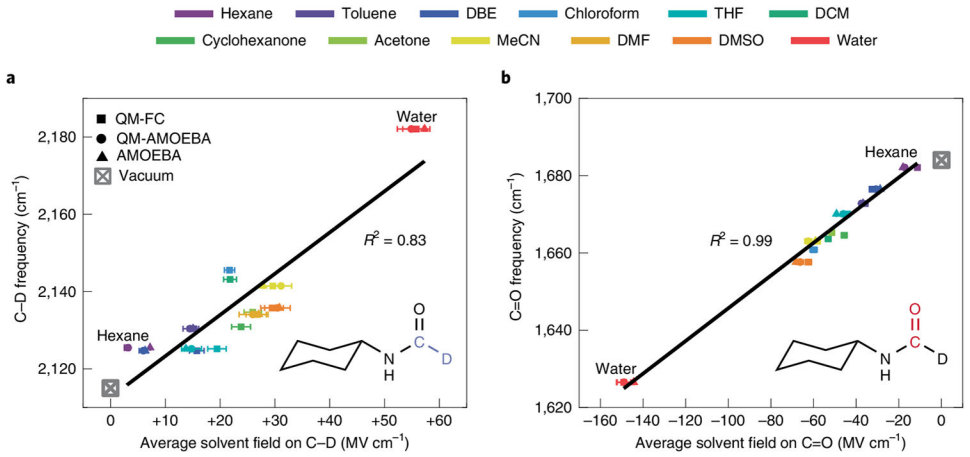

Fig. 4 |. Construction of the field-frequency maps for C—D and C═O in the CXF-D probe using experimentally measured frequency shifts and computed electric field projections along these bonds.

a,b, Field-frequency correlations of C—D **(a)** and C═O **(b)** plotted using the calculated solvent electric fields (ensemble average) and the experimentally measured peak frequencies. Electric fields obtained using three methods are shown and used for the least-squares fits, and additional results can be found in Supplementary Tables 6-13. QM-FC refers to the use of density functional theory and the SPADE electronic structure partitioning scheme[22] (Supplementary Methods) to calculate solvent electric fields based on fixed-charge MD trajectories. QM-AMOEBA refers to the use of the same QM method to calculate the solvent electric fields when based on AMOEBA MD trajectories. AMOEBA refers to the use of the native parameters from the AMOEBA force field, such as the atomic permanent multipoles and polarizabilities, to calculate the solvent electric fields. The error bars represent the standard errors of the solvent field distributions. ‘Vacuum’ shows the results of ab initio harmonic frequency calculations of CXF-D in vacuo at the B3LYP/6-31+G(d,p) level (scaled by 0.964[37]), which serves as a cross-validation of the zero-field case and was not included in the fits. The least-squares regression lines based on the results of all three types of electric field calculations and the measured infrared frequencies are $\nu_{C-D} = 1.07F^{solv}_{C-D} + 2,112.61\,(R^2 = 0.83)$ and $\nu_{C=O} = 0.42F^{solv}_{C=O} + 1,687.97\,(R^2 = 0.99)$, where F^{solv}_{C-D} and $F^{solv}_{C=O}$ denote the projections of the solvent electric fields along the C—D and C═O directions, respectively.

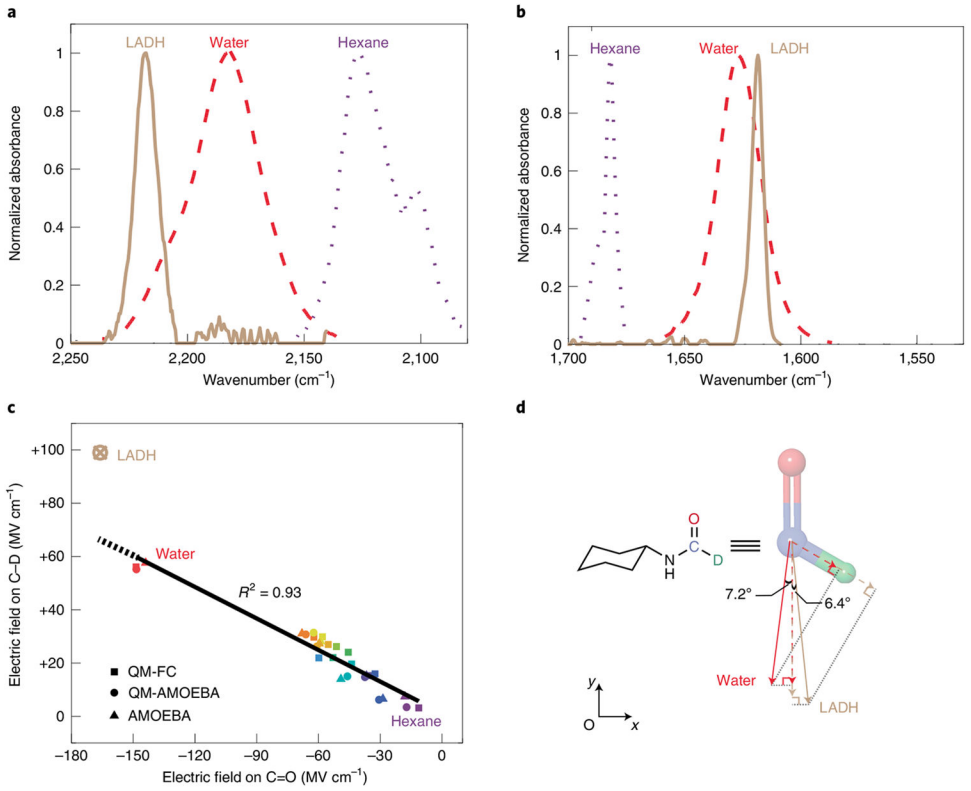

Fig. 5 |. Comparison of the electric field orientations in solvents and at the LADH active site revealed by two-directional electric field measurements.

a,**b**, Normalized infrared spectra of C—D (**a**) and C═O (**b**) with CXF-D bound to the active site of wild-type LADH to form a ternary complex with NADH. The spectra of CXF-D in hexane and water are shown for reference. **c**, Correlation between the average electric fields on C—D and C═O in each solvent (colour code as in Figs. 3 and 4) and LADH. The electric field calculations based on QM-FC, QM-AMOEBA and AMOEBA are as defined in Fig. 4. The least-squares fit does not include the point for LADH, and the result is $F_{C\text{-}D} = -0.39F_{C=O} + 1.21$ ($R^2 = 0.93$) ($R^2 = 0.93$). **d**, Visualization of the electric fields exerted by water (red arrow) and LADH (light brown arrow) based on the results in **c**. The dashed arrows represent the measured electric fields projected on C═O and C—D, from which the orientations of the total electric field on the two-dimensional plane of the aldehyde moiety were obtained (see equation (1)). The solvents exert electric fields of different magnitudes but nearly the same direction: an angle of ~7.2 ± 1.3° with respect to the C═O dipole (the error is based on the slope's standard error in the linear fit). In contrast, the active-site electric field of LADH has a larger magnitude and is oriented in a direction that differs from the direction in the solvents by ~14°.